npj | flexible electronics

Article

Published in partnership with Nanjing Tech University

https://doi.org/10.1038/s41528-026-00550-8

Biodegradable chitosan-cellulose and sub-spherical nanocrystals composite piezoelectric thin film

Check for updates

Valentina Antonaci[1,2] ✉, Gaia de Marzo[2,3] ✉, Laura Blasi[2,4], Virgilio Brunetti[2], Enrico Binetti[2,4], Luca Fachechi[2], Sergio Marras[5], Antonio Qualtieri[2], Francesco Rizzi[2] & Massimo De Vittorio[2,3] ✉

Recently, research has increasingly focused on eco-friendly innovations in sensor and actuator technologies, emphasising the importance of using safe, high-performance, environmentally sustainable, flexible and biocompatible materials in biomedical devices. Our study explores the potential of a composite made of cellulose and chitosan, in developing biodegradable piezoelectric ultrasound transducers. As the piezoelectric technology becomes more common in flexible biomedical devices, the need for sustainable alternatives to traditional synthetic and petroleum-based polymers grows more urgent. The developed biodegradable piezoelectric composites offer a chance to create environmentally friendly solutions that are safe for biological tissues and to support a plastic-free future. By integrating Sub-spherical piezoelectric cellulose nanocrystals CNCs into a chitosan matrix, we significantly improve the piezoelectric properties of flexible thin films. The resulting Chitosan/CNC composite exhibits clear biodegradation under enzymatic hydrolysis conditions and shows a d_{33} value of 30 pC/N comparable to synthetic polymers like polyvinylidene fluoride (PVDF). This enables these films to be processed to produce effective ultrasound transducers, making them promising for various biomedical applications, including non-invasive imaging and wearable health monitoring. These developments represent a significant step toward sustainable, high-performance piezoelectric devices that fulfil the growing needs of next-generation medical technologies.

The search for sustainable and environmentally friendly alternatives to fossil-derived piezoelectric materials has recently accelerated, motivated by the need for safer, biodegradable, and biocompatible technologies[1]. In this context, biopolymer-based piezoelectric devices have emerged as promising candidates for disposable electronics, wearable sensors, and implantable systems, offering a compelling combination of functional performance and ecological safety[2] All these devices exploit the piezoelectric effect that is the generation of a voltage drop across a material under mechanical stress, which produces a deformation of the material lattice and its consequent polarization[3] Since their discovery, piezoelectric materials have been applied across numerous disciplines, with biomedical engineering being one of the most recent prominent areas of utilisation[4] Until now, most of the attention was focused on ceramic-based inorganic materials, like Lead Zirconium Titanate (PZT), which have traditionally been utilised as piezoelectric components in various applications, including sensors[5,6], transducers[6,7] and actuators[8,9] However, their drawbacks include environmental harm, brittleness, and toxicity[10]. In contrast, ceramics such as Barium Titanate ($BaTiO_3$), Zinc Oxide (ZnO) and Aluminium Nitride (AlN) offer improved processability and biocompatibility; however, their piezoelectric efficiency diminishes when processed into thin films[10] Synthetic polymers can serve as a viable alternative to traditional ceramic piezoelectric materials. They offer flexibility and compliance while still performing well in piezoelectric applications. A well-known example is polyvinylidene fluoride (PVDF), which shows excellent piezoelectric coefficient, ranging from 30 to 40 pC/N[11] However, when degraded, since PVDF is derived from fossil sources, produces toxic hydrofluoric acid (HF)[12] To address these limitations, researchers have turned to bio-based piezoelectric materials such as chitosan and cellulose, which are biodegradable, biocompatible, and derived from renewable resources and food waste[13–17] However, their relatively low piezoelectric coefficients and production challenges have hindered their

[1]Department of Innovation Engineering – Università del Salento, Lecce, Italy. [2]Istituto Italiano di Tecnologia – Center for Biomolecular Nanotechnologies, Lecce, Italy. [3]Center IDUN, Department of Health Technology, Technical University of Denmark, Kongens Lyngby, Denmark. [4]CNR-IMM Istituto per la Microelettronica ed i Microsistemi - UOS di Lecce c/o Campus Universitario Ecotekne, Lecce, Italy. [5]Istituto Italiano di Tecnologia—Materials Characterization Facility, Genova, Italy. ✉e-mail: valentina.antonaci@iit.it; gdema@dtu.dk; mdevi@dtu.dk

implementation in thin-film piezoelectric devices[1] Moreover, they exhibit challenges related to irregular surfaces and varying adhesion to substrates[15]. Despite these drawbacks, their unique chemical and mechanical properties make them promising candidates for sustainable microdevices and sensors, such as Microelectromechanical Systems (MEMS) and Piezoelectric Ultrasonic Transducers (UTs)[1,18,19] Chitosan is a biopolymer derived from the exoskeletons of crustaceans and the cell walls of fungi, which can be recovered in significant quantities from the waste of the seafood industry[20] Recently, de Marzo et al. demonstrated the possibility of enhancing the piezoelectric effect of a chitosan thin film through an inexpensive and straightforward chemical treatment, producing a biodegradable piezoelectric thin film suitable for fabricating ultrasonic transducers[21] A promising strategy to further enhance piezoelectric properties involves incorporating nanostructured fillers into biopolymer matrices. While ceramic nanoparticles like $BaTiO_3$ have been used for this purpose[22], attention is now shifting to renewable, biodegradable alternatives such as cellulose nanocrystals (CNCs). CNCs exhibit intrinsic piezoelectric properties and have traditionally been used for mechanical reinforcement[23,24] However, studies on CNCs chitosan films for piezoelectric applications remain limited. Most have employed rod-like CNCs, resulting in piezoelectric sensitivity values significantly lower than PVDF[25].

In this work, we report the fabrication of biocompatible composite film of chitosan and Sub-spherical cellulose nanocrystals (CNCs), which exhibits clear biodegradation under enzymatic hydrolysis conditions and achieves a piezoelectric coefficient (d_{33}) of ~30 pC/N, comparable to PVDF[11,26] This result represents a significant advancement in the field of bio-based piezoelectric materials. Sub-spherical CNCs were selected due to their uniform shape, high surface area, thermal stability, and superior dispersion within the polymer matrix[27] We synthesised Sub-spherical CNCs via sulfuric acid hydrolysis of cellulose powder with diameters ranging from 50 to 200 nm[28,29] The resulting CNCs were freeze-dried and redispersed at five concentrations ranging from 0.3 to 100 mg/ml). These solutions were then added to chitosan in order to obtain Chit-CNC composite films. Afterwards, a free-standing piezoelectric device was fabricated by sandwiching the film between silver and gold electrodes and encapsulating it in Parylene-C. The piezoelectric response of 8×8 mm^2 devices was characterised using a custom-built setup[30], yielding a maximum d_{33} of ~30 pC/N. Additionally, the device demonstrated the ability to detect ultrasound waves, confirming its potential as a biodegradable piezoelectric ultrasonic transducer.

Results

Protocol of extraction and morphological characterisation of cellulose nanocrystals

The extraction was performed according to a protocol described elsewhere[25,27,31]The cellulose nanocrystal (CNCs) preparation began with the dispersion of pure cellulose powder at a concentration of 10% (w/v) in an aqueous solution 55% (v/v) of sulfuric acid (H_2SO_4)[25,31] The mixture was stirred for 50 min at a controlled temperature of 45 °C. Following hydrolysis, the reaction was quenched by dilution with cold water (1:10 v/v). The resulting suspension was centrifuged for 15 min at 10 °C to remove excess sulfuric acid and recover the cellulose nanocrystals as a pellet. The supernatant was then subjected to dialysis using 14 kDa molecular weight cut-off membranes for 24 h to remove residual acid, achieving a final pH of 7. For CNCs drying, the suspension was frozen at -80 °C in Falcon tubes before lyophilisation. The freeze-drying process was conducted under vacuum conditions, with a condenser temperature of -60 °C and a final vacuum of less than 1 mbar, ensuring efficient removal of residual moisture. The resultant dried CNCs were redispersed in ultrapure water for further use (Fig. 1A). The process for producing CNCs is explained more thoroughly in the methods.

We prepared cellulose nanocrystal solutions with defined concentrations (0.3 mg/ml, 3 mg/ml, 15 mg/ml, 30 mg/ml, and 100 mg/ml) by dissolving them in Milli-Q water, allowing for consistent formulations suitable for various applications. SEM provided detailed images of the morphologies of pure cellulose powder (Fig. 1B) and CNCs (Fig. 1C) by using a thin gold coating on samples to enhance conductivity. The images showed that the pure cellulose powder had a fibril structure with particle aggregates, while the CNCs show Sub-spherical nanoparticles having a diameter less than 200 nm with a good dispersion. AFM images revealed Sub-spherical crystals ranging from 50 to 200 nm, indicating a uniform nanocrystal solution with consistent size distribution and minimal agglomeration (Fig. 1D-D'). Analysis of the projected boundary length confirmed the morphological uniformity of the CNCs, showing a narrow distribution of well-defined, non-aggregated particles (Fig. 1D")[25,31–33] Dynamic Light Scattering (DLS) measurements showed a sharp peak between 60 and 70 nm, indicating a narrow size distribution. The DLS findings aligned well with data from scanning electron microscopy (SEM) and AFM, reinforcing the reliability of our results (Fig. 1E). Transmission electron microscopy (TEM) revealed irregular agglomerations and nearly Sub-spherical particles with diameters between 50 nm and 200 nm, consistent with Atomic Force Microscopy (AFM) results (Fig. 1F).

Fabrication and characterisation of the composite Chit-CNC film

Plain chitosan films and composite Chitosan/Cellulose Nanocrystals (CNCs) films were produced to achieve a thickness of approximately 20 μm[21] Chitosan (M.W. 890,000) was dissolved at 1% w/v in a 1% v/v lactic acid aqueous solution, maintaining a slightly acidic pH for complete dissolution. The mixture was stirred for six hours to achieve a uniform, viscous solution. CNC powder was re-dispersed in 100 μl of water at several concentrations (0.3 mg/ml, 3 mg/ml, 15 mg/ml, 30 mg/ml, and 100 mg/ml), and each solution was combined with 40 ml of the chitosan matrix. This led to composites containing CNCs weight percentages of 0.0075%, 0.075%, 0.37%, 0.74%, and 2.4%, resulting in the development of composites termed Chit-CNC-0.3, Chit-CNC-3, Chit-CNC-15, Chit-CNC-30, and Chit-CNC-100, respectively. Fifteen millilitres of Chit-CNC solution was cast in 10 cm Petri dishes and placed in a vacuum oven at 40°C and 200 mbar. After solvent evaporation, the films were treated in 1 M NaOH for 60 min, rinsed until neutralized, and dried overnight. All procedures were conducted in a clean room to avoid contamination (Fig. 2A).

Various analytical methods were used to investigate the interaction between cellulose nanocrystals and the chitosan matrix, focusing on the film's piezoelectric properties. Polarised optical microscope images exhibited morphological alterations with rising CNCs content, particularly a brighter hue (Fig. 2B, C), which suggests a level of anisotropy, a critical characteristic for piezoelectric applications, and a reduction of spherulitic structures, demonstrating CNCs' influence on transcrystallinity[34,35] Birefringence is visible at the edges of the Chitosan/CNC film, especially for Chit-CNC-30 (Fig. 2D), showcasing vibrant iridescent colours that contrast with the subdued colours of the pure chitosan film[36] CNCs facilitate polymer chain ordering by forming a chiral nematic phase at specific concentrations, visible as fingerprint textures under polarized light. Furthermore, fingerprint textures characteristic of chiral nematic ordering were observed in selected samples (Fig. 2E), confirming the self-assembly of CNCs into helicoidal domains[37] This hierarchical organisation, driven by CNCs' concentration, promotes long-range orientational order within the matrix's amorphous regions[38], significantly influencing the composite's optical and piezoelectric properties. The presence and intensity of these chiral nematic structures are strongly dependent on the CNCs dispersion, concentration[39], and interfacial compatibility with the chitosan matrix, highlighting the critical role of CNCs polymer chain interactions in dictating the material's final morphology[40].

X-ray diffraction (XRD) was performed to evaluate the structural organisation of Chitosan/CNC composite films, focusing on how the incorporation of CNCs affects crystallinity[41], which is crucial for piezoelectric performance. All samples displayed two prominent diffraction peaks at 2θ approximately 10° and 20° (Fig. 2F), corresponding to the (020) and (110) crystallographic planes of orthorhombic chitosan ($P2_1P2_1P2_1$), associated with the well-known "Tendon" or "Hydrated" polymorph[42]. The consistent peak positions across varying CNCs concentrations indicate that the orthorhombic crystalline structure of chitosan remains intact with the

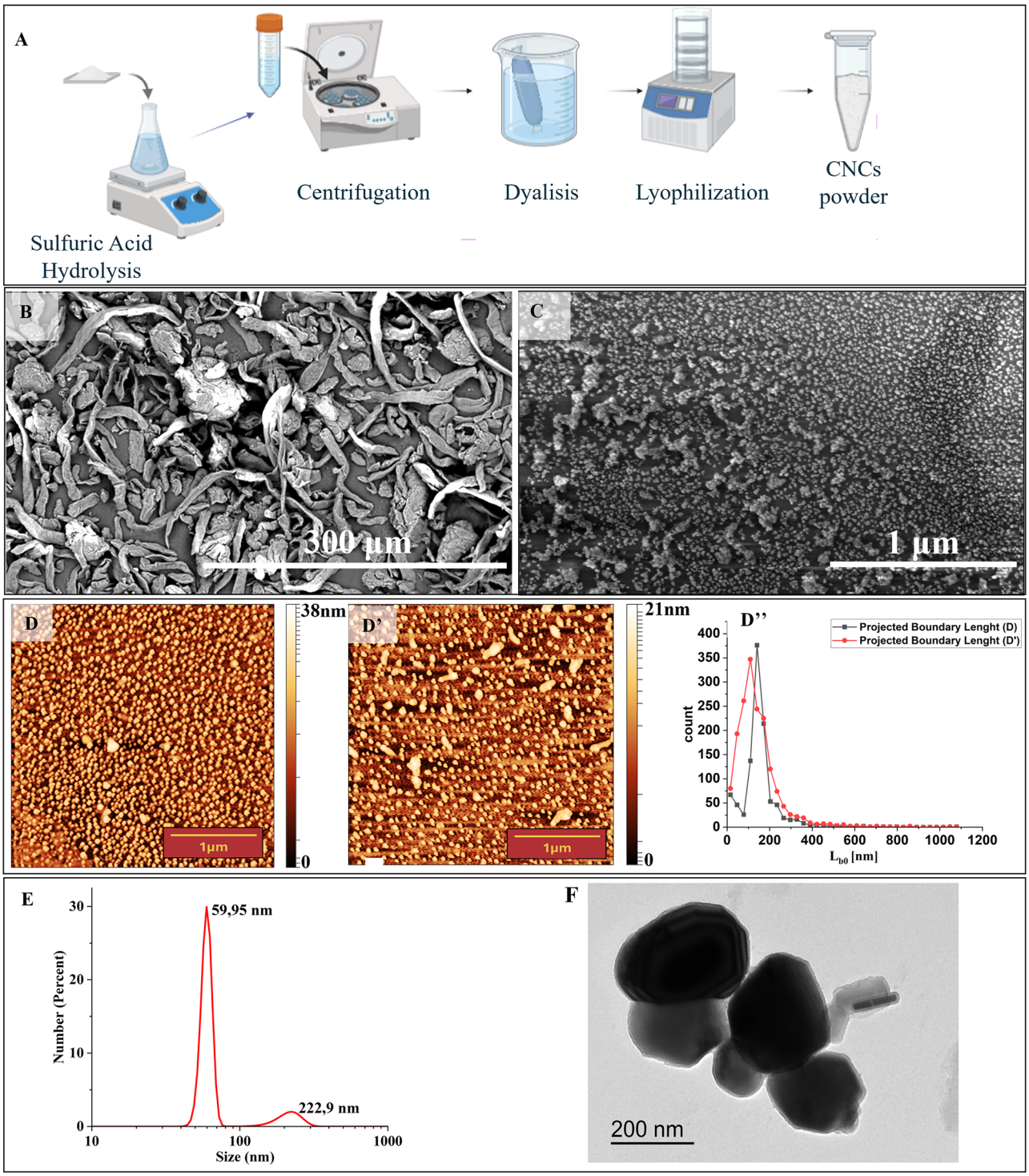

Fig. 1 | Characterization of cellulose nanocrystals (CNCs) and precursor materials. A Illustration of the preparation process of CNCs aqueous suspension. **B** SEM image of raw cellulose powder showing typical fibrous morphology and broad particle distribution. **C** SEM image of CNCs highlighting nanoscale crystalline structure. **D-D'-D"** AFM images of CNCs deposited on glass slide and projected boundary length distribution of CNCs, analysed with Gwyddion software. **E** DLS size distribution by number of CNCs, with a sharp peak at ~65 nm, indicating low polydispersity. **F** TEM images of cellulose nanocrystals (CNCs) produced by Sulfuric acid hydrolysis.

addition of CNCs. These results suggest that CNCs interact preferentially with the amorphous regions.[43,44] of the polymer matrix, promoting transcrystallization,[34] without disrupting the existing crystalline phase. The development of ordered domains and increased structural anisotropy, as seen through polarised optical microscopy (POM), is crucial for affecting the mechanical[45] and piezoelectric properties of the composite film[44]. This highlights the significant role of nanoscale CNCs polymer chain interactions in enhancing functional performance.

Mechanical analysis (Table 1) reveals that Young's modulus decreases with the addition of CNCs, indicating that the chitosan/CNCs blend softens progressively. Although Chit-CNC composites are mechanically softer than pure chitosan, this behavior does not reflect a loss of structural integrity but

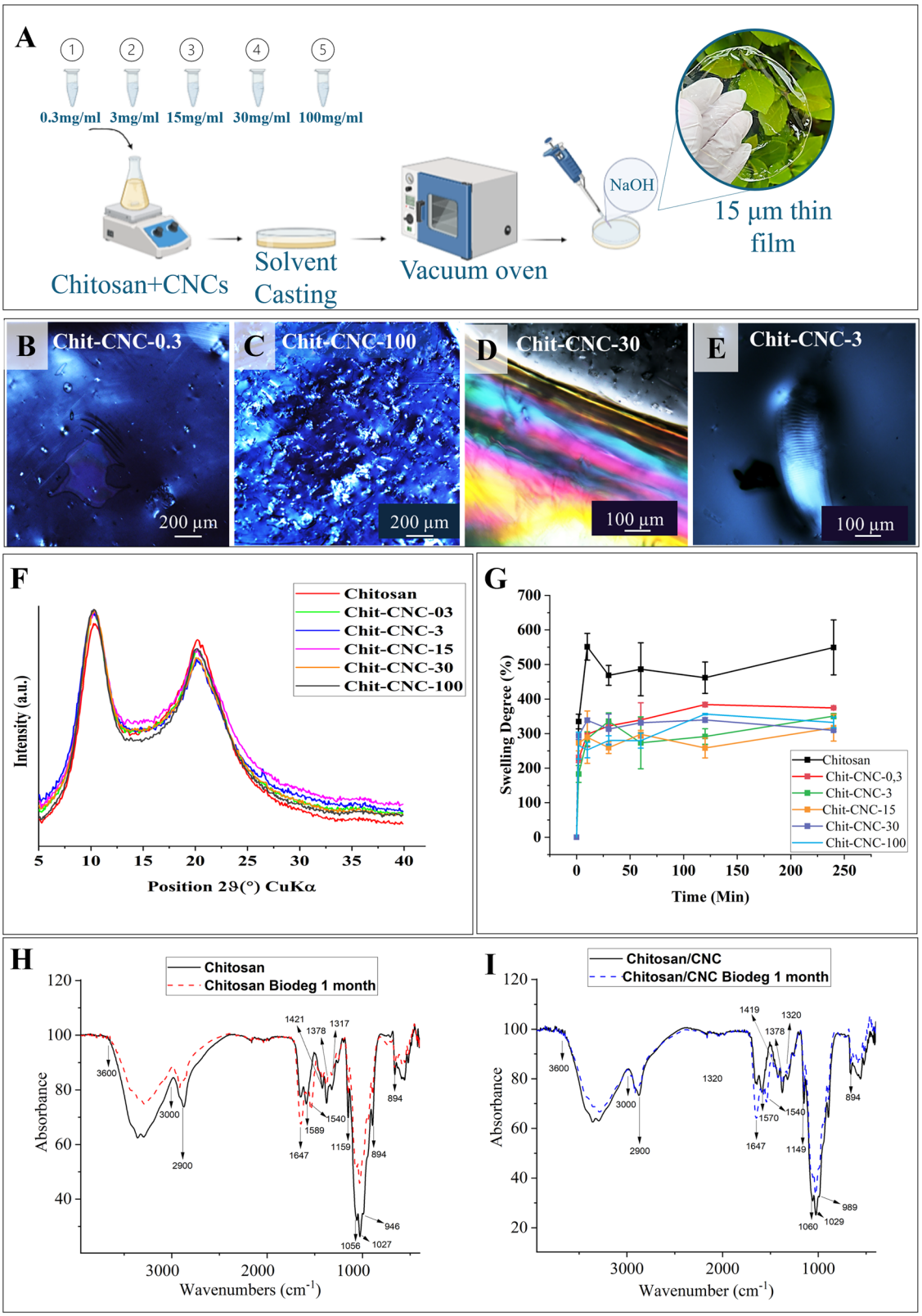

Fig. 2 | Fabrication and characterisation of Chit-CNC composite films. **A** Schematic of Chit-CNC film fabrication: CNC suspension dispersed in chitosan matrix, followed by stirring, solvent casting, and NaOH treatment. Polarised optical microscopy (POM) images of films with (**B**) 0.3 mg/mL **C**) and 100 mg/ml. **D** POM image of film edge (30 mg/mL CNCs). **E** Fingerprint textures in Chit-CNC film (3 mg/mL) **F**) XRD pattern of chitosan and Chit-CNC films at different CNCs concentrations (0.3–100 mg/mL). **G** Swelling degree of pure chitosan and Chit-CNC films. **H** FTIR spectra of chitosan films before and after 1-month biodegradation. *I*) FTIR spectra of Chit-CNC films before and after 1-month biodegradation.

Table 1 | Mechanical properties of pristine and CNCs reinforced chitosan films

Sample	% Cellulose Nanocrystals (mg/ml)	Young Modulus (GPa)
Chitosan	/	2,5
Chit-CNC-0,3	0,3	1,5
Chit-CNC-3	3	1,7
Chit-CNC-15	15	1,1
Chit-CNC-30	30	1,2
Chit-CNC-100	100	1,1

Decreased modulus reflects CNCs-induced mobility in amorphous domains without altering crystalline order.

rather a CNC-induced modulation of the polymer matrix. Specifically, hydrogen bonding and electrostatic interactions at the CNC–chitosan interface regulate local chain mobility and stress transfer.[46,47] The absence of significant changes in the crystalline structure, as evidenced by XRD, suggests that CNCs do not disrupt chitosan crystalline domains. Instead, the combined mechanical and structural data support the interpretation that CNCs predominantly interact with chitosan's amorphous regions[43,44], where they act as nanostructured spacers that modify segmental chain dynamics rather than serving as conventional reinforcing fillers. Consistent with this view, molecular dynamics studies reported in the literature indicate that, while strong interfacial hydrogen bonding enhances CNCs-chitosan adhesion, increased polymer mobility in the vicinity of CNCs surfaces can locally reduce stress transfer unless a sufficiently interconnected network is established[48,49] Accordingly, theoretical frameworks for polysaccharide-based nanocomposites emphasize that uniform CNCs dispersion and controlled local chain rearrangement are necessary to translate such CNCs-induced softening into a stable and functional material response[50] In this context, the observed reduction in Young's modulus can be understood as a manifestation of amorphous-phase modulation, in which CNCs induce localized structural rearrangements while preserving the crystalline integrity of chitosan, leading to a mechanically compliant yet structurally organized composite.

An important aspect to explore when incorporating CNCs into chitosan films is the ability to modulate water interactions for biomedical applications in aqueous environments[51] To evaluate water uptake behaviour, the swelling degree (S) of pure chitosan and chitosan/CNC composite films was determined by monitoring mass variation upon immersion in deionised water at different time points. The swelling degree (S) is calculated using the following Eq. 1:

$$S = \frac{W_f - W_i}{W_i} \text{ X } 100 \quad (1)$$

This analysis directly quantifies water uptake and enables assessment of the films' swelling kinetics. As shown in Fig. 2G, all samples exhibit a rapid initial increase in water absorption followed by the establishment of an equilibrium plateau after approximately 120 min. Compared to neat chitosan, chitosan/CNC composite films show lower water uptake over the entire time range systematically.

The reduced water absorption observed upon CNCs incorporation is attributed to the formation of a more compact and partially crystalline polymer network. Strong hydrogen bonding and intermolecular interactions between CNCs and the chitosan matrix limit chain mobility, reduce the available free volume, and hinder water diffusion within the amorphous regions of the films[35,52].

For the biodegradation experiments, pure Chitosan and Chit-CNC-30 were exposed to chicken egg lysozyme at a concentration of 6 mg/ml in phosphate-buffered saline (PBS). This lysozyme concentration, significantly higher than typical physiological levels, was intentionally selected to establish an accelerated enzymatic degradation protocol, and under these conditions, a one-month degradation period can be considered representative of approximately 3-6 months of degradation under physiological environments. This timeframe is also consistent with the operational lifetime of wearable biomedical devices, which are typically designed for short-term use (days to weeks) and rarely exceed one month[53]Cut into 2×2 mm^2 sections, the films were weighed initially (Wi) and soaked in 5 ml of lysozyme/PBS at 37°C with constant shaking, maintaining a pH of 7[53,54] The films were retrieved, rinsed, dried at 50°C every five days, and weighed again (Wf). After one month, pure Chitosan films showed an average weight loss of 1 mg (from 8 mg to 7 mg), while the Chitosan/CNC composite films lost 0.7 mg (from 10.3 mg to 9.6 mg). FTIR (Fourier Transform Infrared Spectroscopy) analysis investigated the interaction between lysozyme and the materials, elucidating the degradation mechanisms in both film types (Figure H, I). Table 2 summarizes the FTIR spectra of chitosan and Chitosan/CNC. All samples displayed characteristic bands: a broad O–H/N–H stretch (3600–3000 cm^{-1}), C–H stretching of the pyranose ring (~2900 cm^{-1}), amide I (1647 cm^{-1}) and amide II (1589 cm^{-1}), CH_2 bending (1421 cm^{-1}), CH_3 bending (1378 cm^{-1}), amide III (1317 cm^{-1}), glycosidic C–O–C stretching (1159 cm^{-1}), and C–N/C–O stretching (~1056 and 1027 cm^{-1})[53,55–57] After lysozyme treatment, an amide II band at 1540 cm^{-1} appeared in both films, confirming that the chitosan–lysozyme interaction is essential for glycosidic bond degradation[58–60] Post-degradation spectra showed reduced peak intensities, indicating increased molecular flexibility. Composite films retained higher intensities than pure chitosan, suggesting CNCs enhance resistance to enzymatic degradation. A drop of intensity at ~2915 cm^{-1} (C–H stretching, pyranose ring) and ~1153 cm^{-1} (C–O–C stretching) indicates structural changes, including ring opening and glycosidic bond cleavage[61], highlighting CNCs' role in tuning degradation behaviour and preserving film functionality. The limited degradation observed in both cases is probably due to the high deacetylation level of chitosan, which reduces lysozyme's effectiveness since lysozyme mainly targets acetylated polysaccharides[58,62].

Fabrication and piezoelectric characterization of chitosan/CNC transducers

Transducers based on composite Chitosan/CNC piezoelectric material were developed using a protocol modified from a previously published method[21] We fabricated six devices to compare the properties of pure chitosan films with various composites (Chit-CNC-0.3; Chit-CNC-3; Chit-CNC-15; Chit-CNC-30; Chit-CNC-100). The process (Fig. 3A) starts with printing AgCite™ electrodes on a 20 ×20 cm glass substrate using the DragonFly LDM System 3D printer. An interlayer of PEDOT-PSS and glycerol is spin-coated and cured at 140°C for 30 min. Wet Chitosan/CNC films are deposited onto this interlayer, achieving uniform layers through rolling. After drying, the films are peeled off, maintaining the electrode's strong adhesion (Fig. 3D). The resulting freestanding device is flexible, lightweight, and preserves mechanical integrity, making it suitable for conformal or wearable applications (Fig. 3B,C). The top electrode is created by positioning Kapton® masks on the films, then depositing a 10 nm Chromium adhesion layer and a 100 nm gold layer. After removing the masks, electrical connections are added, and the films are encapsulated in a 1 µm-thick Parylene-C layer for protection. Finally, connections are soldered to an electrical board for reliable measurements.

We used a custom-made Piezoelectric Measurement Setup (Fig. 3E) to measure the d_{33} values of soft and thin piezoelectric films[30] The devices tested (Fig. 3B-D) included Pure Chitosan, Chit-CNC-0.3, Chit-CNC-3, Chit-CNC-15, Chit-CNC-30, and Chit-CNC-100, all secured under a speaker on a load cell stage. As illustrated in the device fabrication protocol (Fig. 3A), all devices were coated with a thin parylene layer prior to piezoelectric testing. This coating ensures electrical insulation of the active film and minimized the influence of the environmental factors, such as humidity, during the measurements. A sinusoidal mechanical excitation was applied to the DUT by means of a flat speaker and measured by a load cell. The DUT was preloaded with a steel bar so that the sinusoidal mechanical excitation lies entirely within the measurement range of the load cell. The DUT bottom

Table 2 | FTIR characteristic bands for individual chitosan, biodegraded chitosan, composite chitosan/CNC, and composite chitosan/CNC biodegraded

Band Assignment	Wavenumber (cm^{-1})			
	Chitosan Film	Chitosan Film Biodegradation (1Month)	Chitosan/CNC Film	Chitosan/CNC Film Biodegradation (1Month)
Overlap of O–H and N–H stretching (primary amine)	3360-3290	3360-3290	3355-3284	3355-3284
C–H stretching (pyranose ring)	2915-2897	2915-2897	2919-2873	2919-2873
C = O stretching (amide I)	1647	1647	1648	1648
C = O stretching (amide I)	1647	1647	1647	1647
N–H bending (amide II)	1589	1589	1590	1570
Lysozyme		1540		1540
CH_2 bending (CH_2OH group)	1421	1421	1419	1419
CH_3 bending (n-acetyl group)	1378	1378	1378	1378
C–N stretching (amide III)	1317	1317	1320	1320
C–O–C stretching	1153	1153	1149	1149
C–O stretching C–N stretching	1056-1027-946	1056-1027-946	1060-1029-989	1060-1029-989
C–H bending out of plane	894	894	894	894

electrode is directly connected to ground, whereas an insulated grounded copper tape on top of the DUT was used for electromagnetic shielding the top electrode. The sinusoidal voltage signal from the load cell and the sinusoidal charge signal from the DUT have been measured simultaneously. Applied sinusoidal excitation force is derived from the voltage signal of the load cell. The ratio of the peak-to-peak charge signal to the force signal yields the d_{33} value. The speaker operated at 2 to 10 V, applying increasing force via a grounded copper tape cover. We plotted force on the X-axis and charge on the Y-axis for linear fitting, thereby revealing the piezoelectric coefficients of the devices. Results showed that Pure Chitosan had a d_{33} of 16 ± 2 pC/N, Chit-CNC-0.3 had a d_{33} of 21 ± 3 pC/N, Chit-CNC-3 had 27 ± 2 pC/N, and both Chit-CNC-15 and Chit-CNC-30 showed 30 ± 1 pC/N(Fig. 3E-L). Chit-CNC-100 recorded 30 ± 3 pC/N (Fig. 3I). Composite films with cellulose nanocrystals outperformed pure chitosan film. We observed a correlation between cellulose nanocrystal concentration and piezoelectric performance, reaching a peak d_{33} of 30 pC/N at 15 mg/ml. Beyond this, the d_{33} saturates. Piezoresponse Force Microscopy (PFM) analysis supports these measurements, showing a homogeneous electromechanical response and well-distributed piezoelectric domains within the composite films (Fig. 3O, P). Pure chitosan films have a lower local piezoresponse (15,65 pm V^{-1})[21], while Chit–CNC-30 film reach about 25 pm V^{-1} (Fig. 3Q), aligning with macroscopic d_{33} trends. For this reason, the Chit–CNC–30 formulation was selected for detailed electromechanical analysis, as it exhibits the most stable and reproducible piezoelectric response among the investigated compositions. The slightly lower value compared to the macroscopic d_{33} (~ 30 pC/N) arises from the intrinsic differences between PFM local nanoscale (~500 nm) probing and full-area macroscopic mechanical excitation used in the setup. Additionally, since the cellulose nanocrystals are embedded in the chitosan matrix, it is very challenging to position the PFM tip directly on individual CNCs. In contrast, the custom measurement setup applies a uniform mechanical excitation via a flat speaker, stimulating the full active device area and yielding a value of ~30 pC/N. This enhancement is linked to the mechanical modulation of the chitosan matrix; Dynamic Mechanical Analysis (Table 1) indicates that CNCs predominantly intercalate within the amorphous regions, lowering the Young's modulus and increasing polymer chain mobility[49] By softening the amorphous phase while preserving the crystalline domains, the CNCs facilitate greater local deformation and dipole reorientation[46] a behavior also observed in polymer-based piezoelectric systems[63,64] This increased mechanical compliance, driven by specific interfacial hydrogen-bonding networks between the CNCs and the chitosan matrix, directly promotes the higher piezoelectric responses observed at both the local PFM level and in bulk d_{33} measurements[47,50] Table 3 offers a comparative overview of the piezoelectric coefficients documented in the literature.

Chitosan/CNC devices testing in ultrasonic environment

We conducted ultrasound tests to evaluate the effectiveness of composite Chitosan/CNC devices (Chit-CNC-0.3, Chit-CNC-3, Chit-CNC-15, Chit-CNC-30, Chit-CNC-100) compared to pure chitosan piezoelectric thin films. Experiments were conducted in a water tank to simulate real biological conditions, enhancing ultrasonic wave travel and test sensitivity. Using a custom setup (Fig. 4A), a commercial ultrasound transducer (1 MHz, NTDXducer V303-SU) emitted waves, while a hydrophone served as a reference receiver (Onda, USA). The device under test was positioned between them, stabilized with underwater clamps and moved via an XYZ system for accurate measurements. The emitter was controlled by a pulser/receiver (DPR300 Pulser-Receiver from JSR Ultrasonics) connected to a computer, allowing us to adjust pulse repetition frequency (5 kHz), excitation power (457 V), pulse duration (30-40 ns), and energy output (90.2 μJ). Composite Chitosan/CNC transducer signals were pre-amplified by 36 dB at 1 MHz using a custom wideband amplifier (1 MΩ input impedance), then processed through the pulser/receiver (500Ω input impedance, 30 dB gain) and recorded on an oscilloscope (Tektronix MDO 4104-3). A thin PDMS layer was applied over the device's contacts to enhance alignment with the emitter and protect connections (Fig. 4C). Under the experimental conditions, all composite devices effectively detected the 1 MHz ultrasonic signal. The peak-to-peak voltage (Vp-p) for the Chitosan/CNC samples increased from 1.3 mV (Chit-CNC-0.3) to 25.4 mV (Chit-CNC-3), peaking at 75 mV for Chit-CNC-30 before decreasing to 61 mV for Chit-CNC-100 (Fig. 4D-H). Notably, although the Chit-CNC-100 sample exhibited the highest individual signal recorded (Fig. 4H), its measurements showed a significantly higher standard deviation than the Chit-CNC-30 formulation, indicating lower signal stability and greater variability (Fig. 4B). This trend suggests that higher CNCs concentrations can enhance piezoelectric sensitivity but may also introduce local microstructural heterogeneities, as reflected by increased signal fluctuations. In this context, SEM images of pure chitosan and the composite film (Fig. 4I-N) were captured, providing a reference to assess the impact of CNCs addition. The SEM images of pure chitosan reveal a fairly uniform surface and a dense cross-section morphology. At an intermediate CNCs concentration (Chit-CNC-30), the composite films maintain a homogeneous surface morphology (Fig. 4J) and a compact cross-section

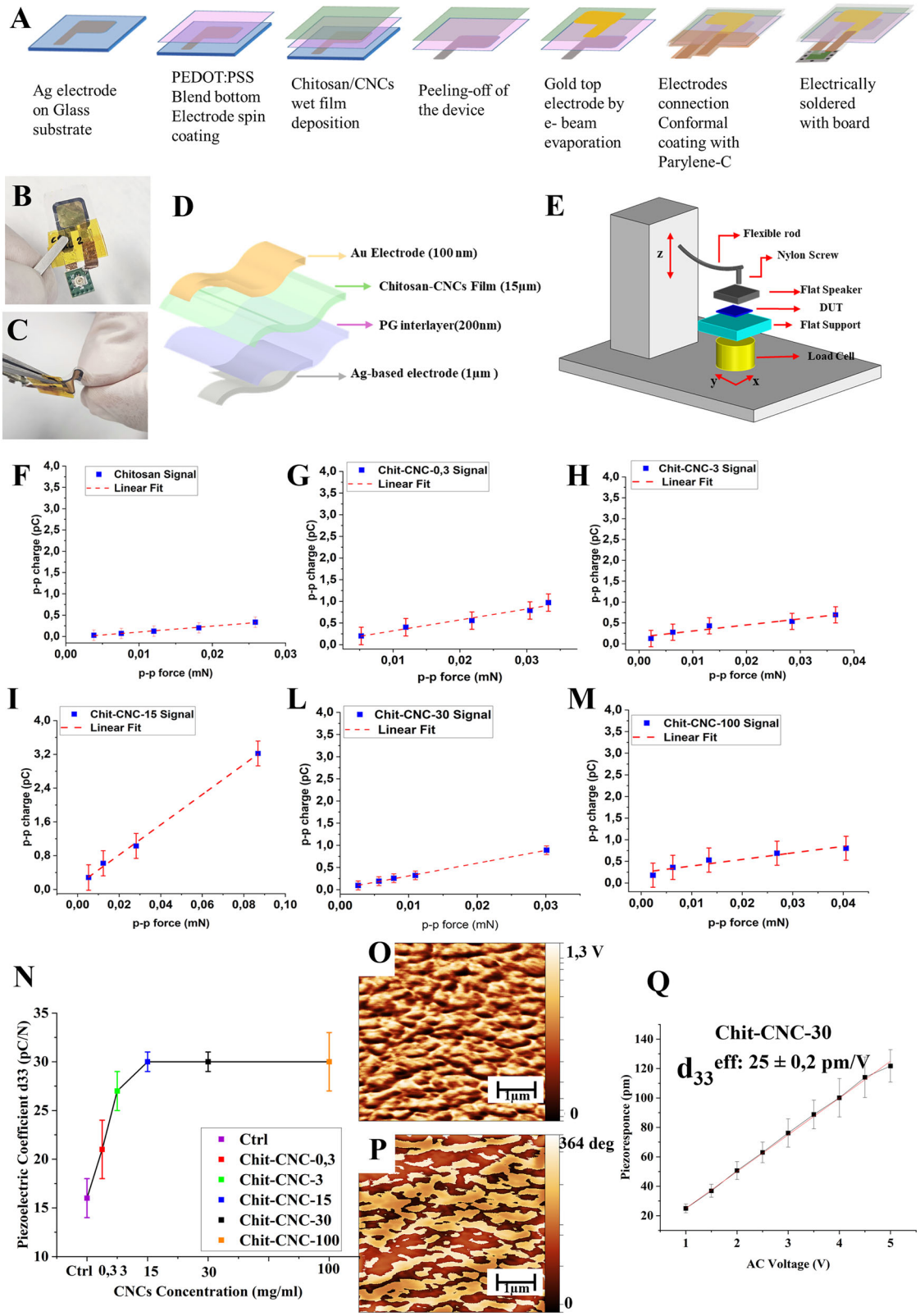

Fig. 3 | High-performance flexible piezoelectric devices based on Chitosan/Cellulose Nanocrystals (CNCs). **A** Fabrication protocol of Chitosan/CNC flags, **B**, **C** Completed device and under bending, demonstrating flexibility, D) Scheme of the device, **E** Schematic representation of the experimental setup for d_{33} measurements. Signals of force and charge generated by (**F**) Chitosan (**G**) Chit-CNC-0,3 H) Chit-CNC-3 (**I**) Chit-CNC-015 (**L**) Chit-CNC-30 (**M**) Chit-CNC-100. **N** Piezoelectric Coefficient (d_{33}) of Chitosan and Chit-CNC devices at different concentrations. (**O**) PFM Amplitude image of Chit-CNC-30 Film. **P** PFM Phase image showing domains distribution in Chit-CNC-30 Film Q) Piezoresponse as a function of applied AC Voltage for the Chit-CNC film, yielding an effective d_{33} of 25 pC/N.

Table 3 | Summary of piezoelectric coefficients reported for chitosan- and cellulose-based films

Composite film material	d_{33} pC/N	Thickness (μm)	Notes	Reference
Chitosan-CNCs (This Work)	30	~15	Free-standing; fully biobased; no ferroelectric fillers;	This Work
Chitosan-PVDF	35	/	Electroactive β-PVDF phase; fluorinated polymer	68
Chitosan/PHB	49,38	/	Biopolymer–synthetic polyester blend; PHB semicrystalline phase	69
Chitosan-$BaTiO_3$	11,24	20-40	Biopolymer matrix with ferroelectric ceramic filler	70
Chitosan-ZnO NPs	65,9	40	Inorganic piezoelectric filler; non-biodegradable component	71
Cellulose/PLLA (Electrospun)	64,2	/	Electrospinning alignment; anisotropic response	43
PEO/H-CNC films	23	35-45	H-bond-induced dipoles	25

(Fig. 4M), indicating an optimal balance between particle dispersion and mechanical coupling. In contrast, at higher CNCs loading (Chit-CNC-100), SEM images reveal less uniform surface features (Fig. 4K) and pronounced microstructural heterogeneities across the film cross-section (Fig. 4N), indicative of reduced structural uniformity and potentially affecting ultrasonic energy transmission efficiency[65,66] This behaviour is consistent with the previously observed saturation of the piezoelectric coefficient at high CNCs concentrations, and may be related to the emergence of locally denser and less homogeneous regions (Fig. 4K) that contribute to the larger signal standard deviation observed for Chit-CNC-100 compared to the more uniform response of Chit-CNC-30. Overall, the results demonstrate that a CNCs concentration of 0.74% significantly improves the detection capabilities of chitosan-based composites with superior signal stability, in agreement with the morphological features observed by SEM.

Discussion

In pursuing a sustainable, plastic-free society and developing biocompatible devices for safely monitoring human health, biodegradable nanomaterials represent an opportunity for enhancing the sensing capabilities of biodegradable devices. Enhancements in piezoelectric characteristics and swelling behaviour aid in developing eco-friendly materials suitable for various applications, specifically biomedical applications, ultimately fostering a greater societal impact. This research presents Cellulose Nanocrystals (CNCs), an entirely biocompatible and biodegradable nanomaterial, as an additive to improve the sensing abilities of piezoelectric thin films made from chitosan. Our findings demonstrate that incorporating CNCs with chitosan notably increases the resulting device's piezoelectric coefficient (d_{33}). The device with 0,74% CNC in the chitosan matrix reached peak d_{33} values of 30 pC/N, showing the most stable, low-noise signal with minimal deviation, comparable to PVDF (30-40 pC/N). Additionally, devices with higher piezoelectric coefficients produced stronger responses to ultrasound amplitudes. These encouraging results underscore the potential of chitosan/CNC composites as entirely biodegradable and eco-friendly piezoelectric ultrasound transducers. Furthermore, this study lays the groundwork for creating sustainable and biocompatible piezoelectric devices for health monitoring and medical uses, such as diagnostic tools and implants that can safely degrade over time. Advancing piezoelectric biodegradable polymers is crucial for developing the next generation of wearable and implantable devices to collect physiological data, encourage tissue regeneration, or deliver targeted therapies. Despite these promising results, challenges related to long-term operational stability, environmental durability, and scalable large-area fabrication remain to be addressed before practical implementation can be achieved.

Methods

Materials

Sulfuric acid (H_2SO_4, 95–98%, Sigma-Aldrich), Dialysis tubing closures and, Dialysis tubing with a molecular weight cut-off of 14 kDa obtained from Sigma-Aldrich, were used for CNCs synthesis. Chitosan (low molecular weight, degree of deacetylation ≥90%, Glentham Life Sciences) and lactic acid (≥85%, Sigma-Aldrich) were employed for film fabrication. Sodium hydroxide (NaOH, Sigma-Aldrich) was used for film neutralisation. For device fabrication, silver nano-ink (Nano Dimension, Israel) was used for bottom electrodes. The mixture PEDOT:PSS high conductivity grade (Sigma-Aldrich) and Glycerol (4% w/w) (Sigma-Aldrich) served as the interlayer. Parylene-C dimer (Speciality Coating Systems) was used for encapsulation. Chicken egg-white lysozyme (Sigma-Aldrich) and phosphate-buffered saline (PBS) (Sigma-Aldrich) were used for the biodegradation test.

Preparation of cellulose nanocrystals (CNCs)

CNCs were obtained by sulfuric acid hydrolysis following well-established protocols.[23–25] Briefly, microcrystalline cellulose (10% w/v) was dispersed in H_2SO_4 (55% v/v, Sigma-Aldrich) and stirred at 45 °C for 50 min. The reaction was quenched with cold deionised water (1:10 v/v), followed by successive centrifugation (6000 rpm, ≈4226 × g, BECKMAN F0685 rotor radius = 10.5 cm,15 min) and dialysis using 14 kDa molecular weight cut-off membranes (Sigma-Aldrich) against water until a neutral pH. The resulting suspension was sonicated using an ultrasonic probe (VCX 750 Vibra-Cell) (225 W, 10 min, ice bath) and stored at 4 °C. For freeze-drying, CNCs suspensions were frozen at −80 °C, lyophilised (ALPHA 1-4 LSC) (−60 °C condenser, vacuum < 1 mbar), and redispersed in water at concentrations of 0.3, 3, 15, 30, and 100 mg mL^{-1}.

Film fabrication

The Chitosan and Composite chitosan/CNCs films were prepared following the methodology described by[21]. Chitosan-based films were prepared by dissolving chitosan in 1% v/v lactic acid under constant stirring. For composite films, 100 μL of CNCs suspensions at varying concentrations were added to 40 mL of the chitosan solution. The mixture was cast onto 10 cm^2 glass Petri dishes and dried overnight at 40 °C under 200 mbar vacuum. Films were then immersed in 1 M NaOH for 1 h, thoroughly rinsed until reaching neutral pH, and air-dried on curved glass substrates. All steps were conducted in a cleanroom environment,

Morphological and structural characterisation

Morphologies of pristine cellulose powder and Cellulose nanocrystals were examined by **Scanning Electron Microscopy** using a dual-beam FIB/SEM (Helios NanoLab 600i, Thermo Scientific). Samples were mounted on aluminium stubs and sputter-coated with a thin layer of gold to improve surface conductivity and prevent charging. Cellulose nanocrystals (CNCs) morphology was analysed by **Atomic Force Microscopy** using a Nano-Observer AFM (CSI) in resonant mode with silicon tips (conductive AppNano FORT silicon tip, 225 μm long, k = 0.6–3.7 N m^{-1}). Samples were prepared by depositing a 20 μl CNCs solution on a glass slide and then drying at 50 °C. **Transmission Electron Microscopy** was performed by drop-casting 20 μl of Cellulose Nanocrystals solution on carbon-coated TEM grids and air-drying overnight. Imaging was performed using a JEOL JEM-1011 microscope. The hydrodynamic diameter of CNCs was measured by **Dynamic Light Scattering (DLS)** using a Zetasizer Nano ZSP (Malvern Instruments). Sonicated suspensions were analysed in disposable cuvettes. Measurements provide an approximation of aggregate size post-

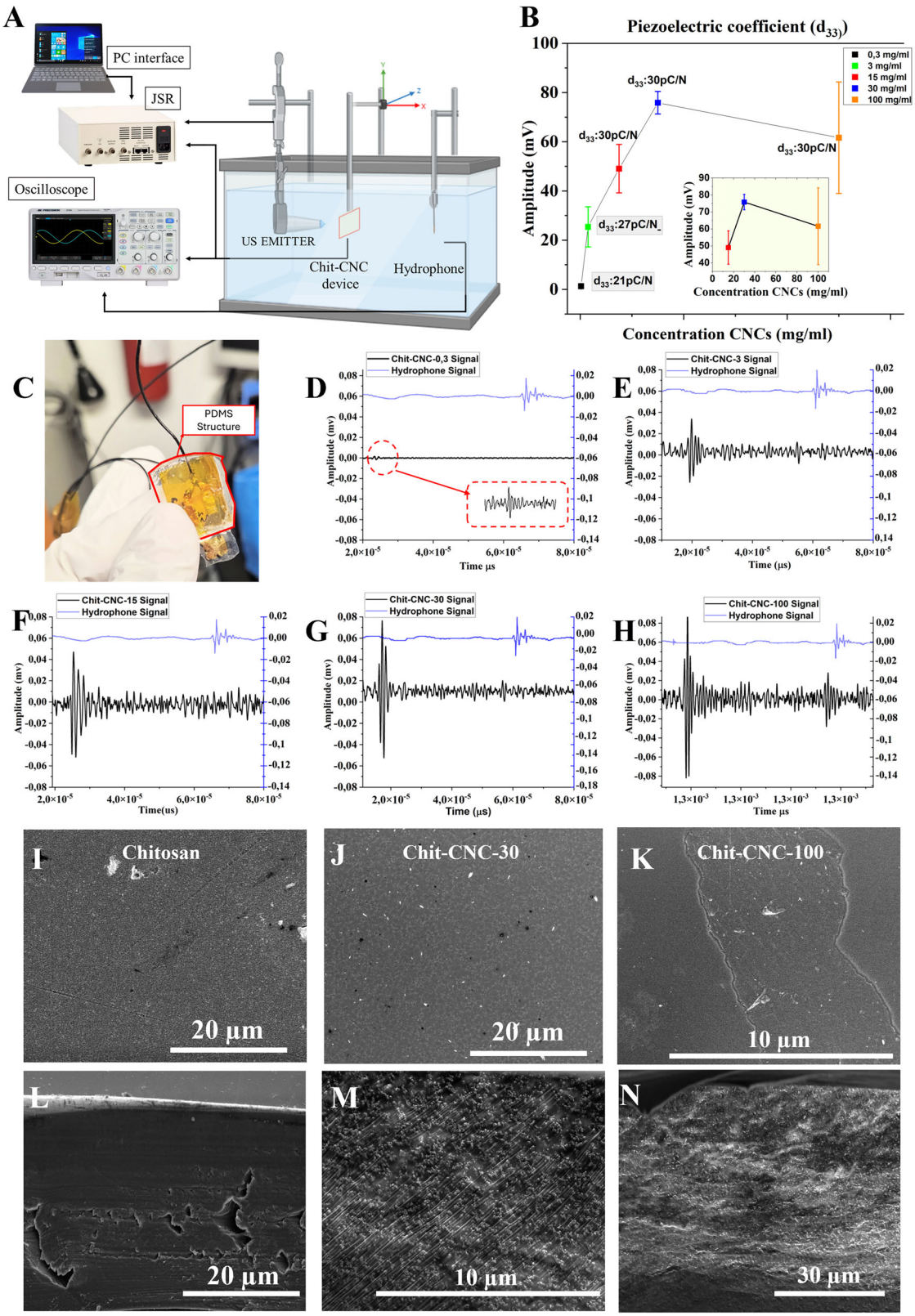

Fig. 4 | Ultrasound sensing performance of Chitosan/Cellulose Nanocrystals (CNCs) piezoelectric devices. A experimental setup for ultrasound sensing, with the XYZ positioning system for precise transducer alignment. **B** Ultrasound signal amplitude of Chitosan/CNC devices with varying CNCs content and corresponding d_{33} values. The inset compares the average ultrasound signals of the devices with 15, 30, and 100 mg/ml CNCs concentrations. Although all three exhibit the same piezoelectric coefficient, the 30 mg/ml device showing the most stable and consistent response. **C** Chitosan/CNC device encapsulated with PDMS for waterproof protection. **D**–**H** Ultrasound signal amplitude recorded by Chitosan/CNC devices with CNC concentrations of 0.3 mg/ml, 3 mg/ml, 15 mg/ml, 30 mg/ml, and 100 mg/ml, respectively. SEM images of (**I**–**K**) flat surfaces and (**L**–**N**) cross-sections of neat chitosan and chitosan/CNC composite films. Neat chitosan (**I**, **L**) and Chit-CNC-30 (**J**, **M**) exhibit relatively uniform surface morphology and compact cross-sections, whereas Chit-CNC-100 (**K**, **N**) shows local microstructural heterogeneities, particularly along the film thickness, consistent with high CNCs loading.

sulfation. Optical anisotropy was evaluated by **Polarised Optical Microscopy (POM)** using a Nikon Eclipse L200NSD microscope equipped with crossed polarisers. **X-ray diffraction (XRD)** analysis was carried out on a Malvern-PANalytical 3rd generation Empyrean X-ray powder diffractometer equipped with a 1.8 kW CuKα X-ray tube operating at 45 kV and 40 mA. The instrument was equipped with iCore and dCore automated PreFIX optical modules and solid-state hybrid pixel PIXcel3D operating in 1D mode. The XRD patterns were collected in air at room temperature, from 2θ = 5° to 40° with a step size of 0.052° using the Bragg-Brentano geometry.

Mechanical test

Tensile tests were carried out using a **Dynamic Mechanical Analyzer (DMA Q800, TA Instruments, USA)**. Chitosan and Chitosan/CNC films were cut into 1 × 6 cm specimens and tested at a constant-force **ramp of 1 N min^{-1}** until failure.

Swelling behavior

Film swelling was evaluated by immersing pre-weighed dry films (W_i) in distilled water (50 mL). At defined time points (2, 10, 30 min, 1, 2, 4 h), samples were removed, blotted with filter paper, and weighed obtaining the final weight (Wf). The swelling ratio (S) (S) is given by the Eq. 1:

$$S = \frac{W_f - W_i}{W_i} \text{ X } 100 \quad (2)$$

Biodegradation tests

To evaluate the biodegradation rate, the sample was incubated in 5 mL of chicken egg-white lysozyme solution (6 mg/mL) prepared in phosphate-buffered saline (PBS, pH 7) at 37°C with constant shaking to ensure even exposure. The biodegradation was tracked over time by periodically measuring the sample's weight changes.

Fourier transform infrared spectroscopy (FTIR)

R spectra were acquired using a JASCO FT/IR6800 spectrometer, equipped with a diamond ATR module. Spectral manipulations were performed using the spectral analysis software from Jasco. Spectra were acquired in the range of 4000–400 cm^{-1} at room temperature on dried samples.

Device fabrication and piezoelectric measurements

Piezoelectric devices were fabricated by sequential deposition of a bottom Ag electrode (1 µm, AgCite™ nanoink, screen-printed), a PEDOT:PSS-glycerol (Sigma-Aldrich) interlayer (200 nm), a 15 µm chitosan/CNC layer, and a top gold electrode (100 nm, e-beam evaporated). Devices were encapsulated with a 1 µm Parylene-C layer. Piezoelectric response was assessed under dynamic mechanical loading using a custom setup applying sinusoidal forces[30].

Piezoresponse force microscopy (PFM)

Glass substrates (300 µm thick, NanoDimension) were cut into 2 × 2 cm² pieces for device fabrication. The bottom electrode was prepared by spin coating a high-conductivity PEDOT:PSS ink (Sigma-Aldrich) blended with glycerol (4 wt%) to enhance conductivity, flexibility, and adhesion.[67] A first PEDOT: PSS/glycerol layer (~200 nm) was spin-coated and cured at 140 °C for 5 min, followed by a second layer cured at the same temperature for 30 min to improve electrical stability. Washed Chit-CN-30 film was transferred onto PEDOT: PSS-coated substrates, leaving part of the electrode exposed, and dried overnight at room temperature. The samples were then cut into 1 × 1 cm² devices, mounted on a magnetic holder, and electrically contacted using silver paste (RS Components). Piezoresponse force microscopy (PFM) measurements were carried out using a Nano-Observer AFM system (CSI Instruments) in contact mode with conductive Pt-coated ANSCM-PC probes (AppNano, spring constant 0.02–0.8 N m^{-1}). An AC voltage of 5 V at ~100 kHz was applied to acquire amplitude and phase signals. The effective piezoelectric coefficient (d_{33}) was determined by calibration against a lithium niobate reference sample.

Ultrasound testing setup

DPR300 Pulser/Receiver (JSR, Japan) and Ultrasound transducer 1 MHz center frequency (NtdXducer, USA) were used as ultrasound origin with pulser at 475 V and 90.2 µJ per pulse. A hydrophone (flat response up to 25 MHz, Onda, USA) was used as a reference. A custom-made amplifier was employed to record the signal from plain chitosan and Chitosan/CNCs device, and both device and hydrophone were connected to the oscilloscope (Tektronix MDO 4104-3) to read ultrasound signals. Measurements were performed in a tank filled with distilled water with devices positioned at different distances from the ultrasound source.

Data availability

The datasets generated and/or analysed during the current study are not publicly available due to their relevance to ongoing research and planned future publications, but are available from the corresponding authors upon reasonable request.

Received: 12 September 2025; Accepted: 10 February 2026;
Published online: 02 March 2026

References

1. Ali, M., Bathaei, M. J., Istif, E., Karimi, S. N. H. & Beker, L. Biodegradable piezoelectric polymers: recent advancements in materials and applications. *Adv. Healthc. Mater.* **12**, e2300318 (2023).
2. Yadegari, A. et al. Recent advancements in bio-based dielectric and piezoelectric polymers and their biomedical applications. *J. Mater. Chem. B* **12**, 5272–5298 (2024).
3. Nagarajan, K. J. et al. A comprehensive review on cellulose nanocrystals and cellulose nanofibers: Pretreatment, preparation, and characterization. *Polym. Compos.* **42**, 1588–1630 (2021).
4. Ji, J. *et al*. Research Trends of Piezoelectric Nanomaterials in Biomedical Engineering. *Adv. Nanobiomed Res*. 3, (2023).
5. Tseng, H. J., Tian, W. C. & Wu, W. J. Flexible PZT thin film tactile sensor for biomedical monitoring. *Sens. (Switz.)* **13**, 5478–5492 (2013).
6. Muralt, P. *et al*. *Piezoelectric Micromachined Ultrasonic Transducers Based on PZT Thin Films*. *2276 ieee transactions on ultrasonics, ferroelectrics, and frequency control* vol. 52 (2005).
7. Cheng, J., Chen, Y., Wu, J. W., Ji, X. R. & Wu, S. H. 3d printing of BaTiO3 piezoelectric ceramics for a focused ultrasonic array. *Sensors (Switzerland)* 19, (2019).
8. Li, J. *et al*. A walking type piezoelectric actuator based on the parasitic motion of obliquely assembled PZT stacks. *Smart Mater. Struct*. 30, (2021).
9. Yuan, H. et al. Low sintering temperature, large strain and reduced strain hysteresis of BiFeO3–BaTiO3 ceramics for piezoelectric multilayer actuator applications. *Ceram. Int.* **47**, 31349–31356 (2021).
10. Habib, M., Lantgios, I. & Hornbostel, K. A review of ceramic, polymer and composite piezoelectric materials. *J. Phys. D. Appl. Phys.* **55**, 423002 (2022).
11. Abbasipour, M., Khajavi, R. & Akbarzadeh, A. H. A comprehensive review on piezoelectric polymeric and ceramic nanogenerators. *Adv. Eng. Mater.* **24**, 2101312 (2022).
12. Zhang, M. et al. Flexible self-powered friction piezoelectric sensor based on structured PVDF-based composite nanofiber membranes. *ACS Appl. Mater. Interfaces* **15**, 30849–30858 (2023).
13. Organic biodegradable piezoelectric materials and their potential applications as bioelectronics. *Soft Science* https://doi.org/10.20517/ss.2022.30 (2023)
14. Wang, R., Sui, J. & Wang, X. Natural piezoelectric biomaterials: a biocompatible and sustainable building block for biomedical devices. *ACS Nano* **16**, 17708–17728 (2022).

15. Zhu, H., Wang, J., Yang, X., Zhang, B. & Wang, Z. Tailoring Biopolymers for Electronic Skins: Materials Design and Applications. *Advanced Materials* 2413112, https://doi.org/10.1002/ADMA.202413112;REQUESTEDJOURNAL:JOURNAL:15214095;WGROUP:STRING:PUBLICATION. (2024).
16. Ansari, M. M., Heo, Y., Do, K., Ghosh, M. & Son, Y. O. Nanocellulose derived from agricultural biowaste by-products–Sustainable synthesis, biocompatibility, biomedical applications, and future perspectives: A review. *Carbohydr. Polym. Technol. Appl.* **8**, 100529 (2024).
17. Yadav, M. et al. Seafood waste: a source for preparation of commercially employable chitin/chitosan materials. *Bioresour. Bioprocess. 2019 6:1* **6**, 1–20 (2019).
18. Li, J., Ma, Y., Zhang, T., Shung, K. K. & Zhu, B. Recent advancements in ultrasound transducer: from material strategies to biomedical applications. *BME Front* **2022**, 9764501 (2022).
19. Xu, M. et al. Piezoelectric biopolymers: advancements in energy harvesting and biomedical applications. *Polym. (Basel)* **16**, 3314 (2024).
20. Agarwal, A., Shaida, B., Rastogi, M. & Singh, N. B. Food packaging materials with special reference to biopolymers-properties and applications. *Chem. Afr. 2022 6:1* **6**, 117–144 (2022).
21. de Marzo, G. *et al*. Sustainable, flexible, and biocompatible enhanced piezoelectric chitosan thin film for compliant piezosensors for human health. *Adv. Electron. Mater*. 9, (2023).
22. Fathollahzadeh, V. & Khodaei, M. Enhanced piezoelectric response of PVDF by incorporating of BaTiO3 nanoparticles and surface treatment. *J. Mater. Sci.: Mater. Electron.* **35**, 1–16 (2024).
23. Bettotti, P. & Scarpa, M. Nanocellulose and Its Interface: On the Road to the Design of Emerging Materials. *Adv. Mater. Interfaces* 9, (2022).
24. Teodoro, K. B. R. et al. A review on the role and performance of cellulose nanomaterials in sensors. *ACS Sens* **6**, 2473–2496 (2021).
25. Miao, C., Reid, L. & Hamad, W. Y. Moisture-tunable, ionic strength-controlled piezoelectric effect in cellulose nanocrystal films. *Appl. Mater. Today* 24, (2021).
26. Liu, S., Qamar, S. A., Qamar, M., Basharat, K. & Bilal, M. Engineered nanocellulose-based hydrogels for smart drug delivery applications. *Int. J. Biol. Macromol.* **181**, 275–290 (2021).
27. Do, T. V. V., Tran, N. B. A. & Nguyen-Thai, N. U. Preparation of spherical nanocellulose from <scp>Gai</scp> bamboo and mechanical properties of chitosan/nanocellulose composite. *Polym. Compos.* **44**, 2287–2295 (2023).
28. Lin, N. & Dufresne, A. Surface chemistry, morphological analysis and properties of cellulose nanocrystals with gradiented sulfation degrees. *Nanoscale* **6**, 5384–5393 (2014).
29. Moon, R. J., Martini, A., Nairn, J., Simonsen, J. & Youngblood, J. Cellulose nanomaterials review: structure, properties and nanocomposites. *Chem. Soc. Rev.* **40**, 3941–3994 (2011).
30. de Marzo, G. et al. On the measurement of piezoelectric d33 coefficient of soft thin films under weak mechanical loads: A rapid and affordable method. *Mater. Des.* **247**, 113399 (2024).
31. Di Giorgio, L., Martín, L., Salgado, P. R. & Mauri, A. N. Synthesis and conservation of cellulose nanocrystals. *Carbohydr. Polym.* **238**, 116187 (2020).
32. Shakouri, Z., Nazockdast, H. & Sadeghi Ghari, H. Effect of the geometry of cellulose nanocrystals on morphology and mechanical performance of dynamically vulcanized PLA/PU blend. *Cellulose* **27**, 215–231 (2020).
33. Al-haql, M., Habbal, H., Al Oklah, B. & Qurabi, N. Extraction and characterization of spherical nanocellulose from sesame husks. *Heliyon* **11**, e41269 (2025).
34. Ahmad, N. D., Kusmono & Wildan, M. W. Preparation and properties of cellulose nanocrystals-reinforced Poly (lactic acid) composite filaments for 3D printing applications. *Results Eng.* **17**, 100842 (2023).
35. Kusmono Wildan, M. W. & Lubis, F. I. Fabrication and Characterization of Chitosan/Cellulose Nanocrystal/Glycerol Bio-Composite Films. *Polymers 2021, Vol. 13, Page 1096* 13, 1096 (2021).
36. Wojno, S., Fazilati, M., Nypelö, T., Westman, G. & Kádár, R. Phase transitions of cellulose nanocrystal suspensions from nonlinear oscillatory shear. *Cellulose* **29**, 3655–3673 (2022).
37. Gray, D. G. et al. Chiral nematic structure of cellulose nanocrystal suspensions and films; polarized light and atomic force microscopy. *Mater* **8**, 7873–7888 (2015).
38. Chen, J. et al. All bio-based chiral nematic cellulose nanocrystals films under supramolecular tuning by chitosan/deacetylated chitin nanofibers for reversible multi-response and sensor application. *Chem. Eng. J.* **466**, 143148 (2023).
39. Korolovych, V. F. et al. Cellulose nanocrystals with different morphologies and chiral properties. *Polym. (Guildf.)* **145**, 334–347 (2018).
40. Miao, C. & Hamad, W. Y. Critical insights into the reinforcement potential of cellulose nanocrystals in polymer nanocomposites. *Curr. Opin. Solid State Mater. Sci.* **23**, 100761 (2019).
41. Li, H. Z., Chen, S. C. & Wang, Y. Z. Preparation and characterization of nanocomposites of polyvinyl alcohol/cellulose nanowhiskers/chitosan. *Compos. Sci. Technol.* **115**, 60–65 (2015).
42. Aranaz, I. et al. Chitosan: an overview of its properties and applications. *Polym. 2021, Vol. 13, Page 3256* **13**, 3256 (2021).
43. Xu, L. *et al*. Fully biodegradable piezoelectric nanogenerator based on cellulose/PLLA electrospun fibers with high-performance for mechanical energy harvesting. *Colloids Surf. A Physicochem. Eng. Asp*. 706, (2025).
44. Xiao, X. et al. Tunable Construction of Chiral Nematic Cellulose Nanocrystals/ZnO Films for Ultra-Sensitive, Recyclable Sensing of Humidity and Ethanol. *Int. J. Mol. Sci. 2024, Vol. 25, Page 4978* **25**, 4978 (2024).
45. Khan, A. et al. Mechanical and barrier properties of nanocrystalline cellulose reinforced chitosan based nanocomposite films. *Carbohydr. Polym.* **90**, 1601–1608 (2012).
46. Luo, Y. et al. Chitosan particles modulate the properties of cellulose nanocrystals through interparticle interactions: Effect of concentration. *Int. J. Biol. Macromol.* **240**, 124500 (2023).
47. Riva, G. H. et al. Cellulose - chitosan nanocomposites - evaluation of physical, mechanical and biological properties. *Cellul. - Fundamental Asp. Curr. Trends* https://doi.org/10.5772/61727 (2015).
48. Zheng, X., Yang, H., Xia, W. & Zhang, Y. Size-dependent mechanical behaviors of cellulose nanocrystals induced by interfacial zone: implications for advanced electronic devices design. *ACS Appl. Nano Mater.* **8**, 3974–3984 (2025).
49. Zheng, X., Li, Y., Xu, S., Yang, H. & Zhang, Y. Interfacial mechanical behavior of cellulose nanocrystals and chitosan. *Macromolecules* **58**, 803–815 (2024).
50. Marin, L. & Bardosova, M. Functional Chitosan-Based Composites. *Functional Chitosan-Based Composites* 200 https://doi.org/10.3390/BOOKS978-3-0365-4649-0. (2022).
51. Ghasemlou, M., Daver, F., Ivanova, E. P., Murdoch, B. J. & Adhikari, B. Use of synergistic interactions to fabricate transparent and mechanically robust nanohybrids based on starch, non-isocyanate polyurethanes, and cellulose nanocrystals. *ACS Appl. Mater. Interfaces* **12**, 47865–47878 (2020).
52. Yadav, M., Behera, K., Chang, Y. H. & Chiu, F. C. Cellulose nanocrystal reinforced chitosan based UV barrier composite films for sustainable packaging. *Polym. 2020, Vol. 12, Page 202* **12**, 202 (2020).
53. Reay, S. L., Jackson, E. L., Ferreira, A. M., Hilkens, C. M. U. & Novakovic, K. In vitro evaluation of the biodegradability of chitosan–genipin hydrogels. *Mater. Adv.* **3**, 7946–7959 (2022).
54. Hashemi Doulabi, A., Mirzadeh, H., Imani, M. & Bagheri-Khoulenjani, S. Chitosan/polyethylene glycol fumarate blend films for wound

dressing application: in vitro biocompatibility and biodegradability assays. *Prog. Biomater.* **7**, 143–150 (2018).
55. Frick, J. M., Ambrosi, A., Pollo, L. D. & Tessaro, I. C. Influence of glutaraldehyde crosslinking and alkaline post-treatment on the properties of chitosan-based films. *J. Polym. Environ.* **26**, 2748–2757 (2018).
56. Islam, N., Wang, H., Maqbool, F. & Ferro, V. In vitro enzymatic digestibility of glutaraldehyde-crosslinked chitosan nanoparticles in lysozyme solution and their applicability in pulmonary drug delivery. *Molecules* **24**, 1271 (2019).
57. Altun, E., Çelik, E. & Ersan, H. Y. Tailoring the microbial community for improving the biodegradation of chitosan films in composting environment. *J. Polym. Environ.* **28**, 1548–1559 (2020).
58. Lončarević, A., Ivanković, M. & Rogina, A. Lysozyme-induced degradation of chitosan: the characterisation of degraded chitosan scaffolds. *J. Tissue Repair Regeneration* **1**, 12–22 (2017).
59. Guarino, V. et al. Degradation properties and metabolic activity of alginate and chitosan polyelectrolytes for drug delivery and tissue engineering applications. *AIMS Mater. Sci.* **2**, 497–502 (2015).
60. Roman, D. L., Ostafe, V. & Isvoran, A. Deeper inside the specificity of lysozyme when degrading chitosan. A structural bioinformatics study. *J. Mol. Graph. Model.* **100**, 107676 (2020).
61. Ramírez-Hernández, A. et al. Fingerprint analysis of FTIR spectra of polymers containing vinyl acetate. *Dyna (Medellin)* **86**, 198–205 (2019).
62. Makrani, N., Ammari, A., Benrekaa, N., Rodrigue, D. & Giroux, Y. Dynamics of the α-relaxation during the crystallization of PLLA and the effect of thermal annealing under humid atmosphere. *Polym. Degrad. Stab.* **164**, 90–101 (2019).
63. Ren, K., Shen, Y. & Wang, Z. L. Piezoelectric Properties of Electrospun Polymer Nanofibers and Related Energy Harvesting Applications. *Macromol. Mater. Eng.* **309**, https://doi.org/10.1002/mame.202300307 (2024).
64. Zhao, G. et al. Electrospun Poly(l-Lactic Acid) Nanofibers for Nanogenerator and Diagnostic Sensor Applications. *Macromol. Mater. Eng.* **302**, https://doi.org/10.1002/mame.201600476 (2017).
65. Shojaeiarani, J., Bajwa, D. S., Stark, N. M. & Bajwa, S. G. Rheological properties of cellulose nanocrystals engineered polylactic acid nanocomposites. *Compos. B Eng.* **161**, 483–489 (2019).
66. Lu, T. et al. Effects of modifications of bamboo cellulose fibers on the improved mechanical properties of cellulose reinforced poly(lactic acid) composites. *Compos. B Eng.* **62**, 191–197 (2014).
67. Yamaguchi, H. et al. Highly flexible and conductive glycerol-doped PEDOT:PSS films prepared under an electric field. *J. Electron. Mater.* **47**, 3370–3375 (2018).
68. Zhou, S. et al. Chitosan-Doped PVDF film with enhanced electroactive β phase for piezoelectric sensing. *ACS Appl. Electron. Mater.* **6**, 2575–2583 (2024).
69. Sun, S. et al. Thermoplastic PHB-reinforced chitosan piezoelectric films for biodegradable pressure sensors. *ACS Appl. Bio Mater.* **7**, 6823–6831 (2024).
70. Prokhorov, E. et al. Chitosan-BaTiO3 nanostructured piezopolymer for tissue engineering. *Colloids Surf. B Biointerfaces* **196**, 111296 (2020).
71. Prokhorov, E., Luna-Bárcenas, G., Limón, J. M. Y., Sánchez, A. G. & Kovalenko, Y. Chitosan-ZnO nanocomposites assessed by dielectric, mechanical, and piezoelectric properties. *Polym. 2020, Vol. 12, Page 1991* **12**, 1991 (2020).

Acknowledgements

The authors thank Dr Riccardo Di Corato and the Unisalento/CNR joint-lab "NanoBioelectronics, NanoBiotechnology and Nanomedicine Facility (N3-LAB)" for the support in FT-IR measurements. The authors thank Dr Luciana Algieri and the Unisalento/ CBN-IIT joint lab "Advanced BioInterface Technologies Lab" for supporting the Gwyddion analysis of AFM images. This research has been supported by Novo Nordisk Foundation (grant number NNF23OC0079433).

Author contributions

V.A. designed the study, performed data analysis, curated the results, prepared the figures, and wrote the original draft. G.d.M. contributed to conceptualisation and methodology, supported the data analysis, and contributed to validation, writing, review and editing. L.B. contributed to validation and writing, review, and editing. V.B., E.B., L.F., S.M., and A.Q. performed measurements and contributed to data acquisition. F.R. contributed to validation and writing, review, and editing. M.D.V. supervised the research, validated the findings, and contributed to writing, review and editing. All authors reviewed and approved the final version of the manuscript.

Competing interests

The authors declare no competing interests.

Additional information

Correspondence and requests for materials should be addressed to Valentina Antonaci, Gaia de Marzo or Massimo De Vittorio.

Reprints and permissions information is available at http://www.nature.com/reprints

Publisher's note Springer Nature remains neutral with regard to jurisdictional claims in published maps and institutional affiliations.

Open Access This article is licensed under a Creative Commons Attribution-NonCommercial-NoDerivatives 4.0 International License, which permits any non-commercial use, sharing, distribution and reproduction in any medium or format, as long as you give appropriate credit to the original author(s) and the source, provide a link to the Creative Commons licence, and indicate if you modified the licensed material. You do not have permission under this licence to share adapted material derived from this article or parts of it. The images or other third party material in this article are included in the article's Creative Commons licence, unless indicated otherwise in a credit line to the material. If material is not included in the article's Creative Commons licence and your intended use is not permitted by statutory regulation or exceeds the permitted use, you will need to obtain permission directly from the copyright holder. To view a copy of this licence, visit http://creativecommons.org/licenses/by-nc-nd/4.0/.

© The Author(s) 2026